Wide-angle X-ray studies on ethylene–tetrafluoroethylene (ETFE) copolymers

T. Pieper, B. Heise and W. Wilke*

Abteilung Experimentelle Physik, Universität Ulm, Oberer Eselsberg, D-7900 Ulm, FRG

(Received 10 February 1988; revised 2 December 1988; accepted 27 January 1989)

The orientation parameters $\langle P_2 \rangle$ of the chain segments in the amorphous layers of uniaxially drawn ethylene–tetrafluorethylene (ETFE) copolymers with different side chain modifications were determined from the separated amorphous halo of wide angle X-ray scattering (WAXS) measurements. The orientation distribution of the crystallographic axes in the 'crystal' domains, which show essentially a two-dimensional order in lateral direction, was obtained from the analysis of *hk*0 reflections. The crystal orientation is independent of the side chain modifications. Both the mean lattice constant and the mean extension of the coherent scattering domains were determined to be temperature-dependent using synchrotron radiation. The anomaly of these parameters at about 100°C is attributed to a transition of the crystal structure.

(Keywords: WAXS; crystal orientation; segment orientation; two-dimensional order; transition)

INTRODUCTION

Ethylene–tetrafluoroethylene (ETFE) is known to have similar properties to polytetrafluoroethylene (PTFE), i.e. high chemical and ageing resistance as well as good mechanical and electrical properties. In contrast to PTFE, ETFE is suitable for extrusion applications because its melt viscosity is much smaller. ETFE is used for electrical insulation purposes, as washer material and for chemical applications[1,2].

ETFE represents a model system of semicrystalline polymers having good long-range order within the crystals in lateral direction of the molecules but poor order in chain direction. The periodicity in chain direction is disturbed by the irregular alternating order of CH_2 and CF_2 groups within the chains on the one hand and by longitudinal displacement of the chains themselves on the other hand. Therefore, in an X-ray diffraction measurement only strong *hk*0 and 00*l* reflections appear; *hkl* reflections are very weak. In this paper the two main diffraction peaks (120 and 200) of wide angle X-ray scattering (WAXS) measurements on various ETFE samples were separated from the amorphous halo by a numerical technique. The orientation behaviour of both crystalline and amorphous regions will be discussed by means of the azimuthal distribution of the *hk*0 reflections and the amorphous halo respectively. As a by-product of the separation procedure, crystallinity and lattice constants were determined.

EXPERIMENTAL

Samples

All samples were extracted from moulded granulated material using a hydraulic pressing device and were heated at about 300°C under pressure of 0.8 MPa. The plate material produced in this way was punched into dumb-bell shaped specimens and tested for isotropy with the X-ray diffractometer described below. The oriented samples were prepared at room temperature using a conventional tensile testing machine. The strain rate varied from $\dot{\lambda}=0.03\,\text{min}^{-1}$ to $\dot{\lambda}=0.05\,\text{min}^{-1}$ with respect to the initial length. The chemical compositions and the densities are listed in *Table 1*.

X-ray measurements

The X-ray diffraction data of all oriented samples were taken on a computer-controlled two-circle counter diffractometer (Philips PW 1078/25) using Ni-filtered Cu–Kα radiation. In order to keep the reciprocal space vector parallel to the sample plane, all measurements were taken with symmetrical transmission geometry (*Figure 1*). The diffraction data of the unoriented ETFE copolymers were obtained with monochromatic synchrotron radiation ($\lambda=0.150\,\text{nm}$) while heating the sample continuously in a special heating device. The heating rate was 10 K/min. The calibration of the Q scale was effected

Table 1 Chemical compositions and densities of samples A–G. Abbreviations: E, ethylene: $[CH_2]_2$; TFE, tetrafluoroethylene: $[CF_2]_2$; HFP, hexafluoropropylene: $CF_2=CF-CF_3$; PPVE, perfluoropropyl-vinyl-ether; $CF_3-[CF_2]_3-O-CF=CF_2$; HFIB, hexafluoroisobutene: $CF_3-\underset{\underset{CH_2}{\|}}{C}-CF_3$

Sample	Chemical composition (mol%) (E/TFE/HFP/PPVE)	Density (g/cm^3)
Bip A	53.5/46.5/ – / –	1.668
Bip B	45.1/54.9/ – / –	1.757
Qua C	45.7/52.8/1.0/0.5	1.718
Qua D	49.3/48.0/2.3/0.4	1.702
Ter E	48.5/47.5/4.0/ –	1.731
Qua F	49.0/46.2/4.3/0.5	1.743
Ter G	? /? /5.8 HFIB	1.726

* To whom correspondence should be addressed

0032-3861/89/101768-08$03.00

using the (111) reflection of silicon and the (011) reflection of $CaWO_4$.

Intensity corrections and estimate of error

The diffraction data was corrected with respect to instrumental background, absorption, Compton scattering, polarization and multiple scattering[3–5]. In order to estimate the errors of the orientation parameters caused by instrumental broadening, the influence of the primary beam divergence (approximately 1 degree) on the azimuthal deviation of the scattering vector was calculated using the geometrical dimensions of our diffractometer. The resulting deviation was $\Delta\varphi/2 = 3.04$ degrees.

The intensity I measured by the detector with respect to azimuthal terms is given by

$$I_{ex}(\varphi) = (1/\Delta\varphi) \int_{\varphi-(\Delta\varphi/2)}^{\varphi+(\Delta\varphi/2)} I(\psi)\mathrm{d}\psi \qquad (1)$$

See *Figure 1* for angle φ.

Then, $\langle\cos^2\varphi\rangle$ has been calculated by expanding $I(\psi)$ into Taylor series up to terms of second order. The result is

$$\langle\cos^2\varphi\rangle = \frac{\int_0^{\pi/2} \cos^2\varphi[I(\varphi) + \frac{(\Delta\varphi)^2}{24} I''(\varphi)] \sin\varphi \, \mathrm{d}\varphi}{\int_0^{\pi/2} [I(\varphi) + \frac{(\Delta\varphi)^2}{24} I''(\varphi)] \sin\varphi \, \mathrm{d}\varphi} \qquad (2)$$

In comparison with the well known formula of $\langle\cos^2\varphi\rangle$ the second derivative of $I(\varphi)$ appears. If the intensity distribution $I(\varphi)$ is smooth, i.e. if it shows no marked maxima, $I''(\varphi)$ is small compared with $I(\varphi)$ and can be neglected.

In our measurements the influence of the primary beam divergence on the final values of orientation parameters and crystallinities is in the order of 10^{-4}. The uncertainty of those values is determined mainly by statistical errors of the separation procedures in the order of 5%.

THEORY

Separation procedure

In order to determine the orientation behaviour of the 'crystals' and the chain segments within the amorphous layers it is necessary to separate the 'crystal' reflections from the amorphous halo in a reproducible manner. In this work we used the following numerical separation procedure.

The scattering curve is fitted by an analytical function consisting of a sum of Lorentzian squared profiles. We found that this is a good approximation for the 'crystal' reflections by testing Pearson type VII distributions[6] of the form

$$I(Q) = I_0 \Big/ \left[1 + \frac{(Q-Q_0)^2}{ma^2}\right]^m \qquad (3)$$

where: $Q = |\underline{Q}| = 2\pi \times (2\sin\theta/\lambda)$; $\underline{Q} = \underline{k}_s - \underline{k}_0$ (see *Figure 1*); 2θ is the scattering angle and λ is the wavelength.

Figure 2 shows how the variation of m influences the form of the distribution.

$m = 2$ (Lorentzian squared) was used throughout this work to fit both crystal reflections and the amorphous halo. In *Figure 3* an example of the separation of $hk0$-reflections from the amorphous halo is shown.

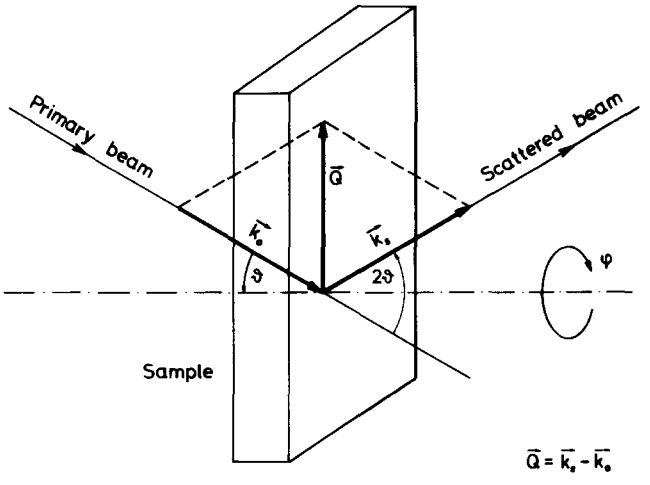

Figure 1 Symmetrical transmission geometry

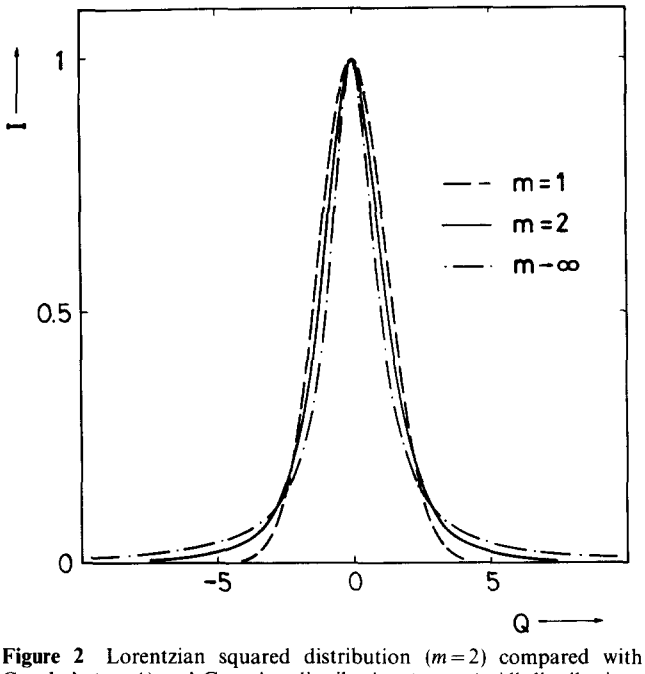

Figure 2 Lorentzian squared distribution ($m=2$) compared with Cauchy's ($m=1$) and Gaussian distribution ($m\to\infty$). All distributions are normalized to equal area

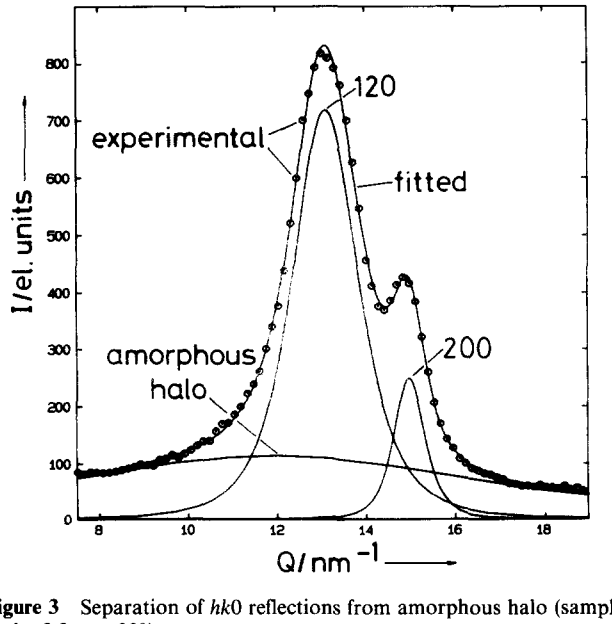

Figure 3 Separation of $hk0$ reflections from amorphous halo (sample B, $\lambda = 2.2$, $\varphi = 90°$)

Orientation of chain segments within amorphous layers

For the description of the atomic distribution in an amorphous solid or in a fluid it is common to introduce the atomic density correlation function (DCF) $\hat{\rho}_a(\underline{R})$. It indicates the probability of finding two atoms with the distance $\underline{R}$ to each other, integrated over the whole sample volume. In an X-ray measurement only the Fourier transform of the electronic DCF can be seen. Therefore, the atomic and the electronic DCF $\hat{\rho}_e(\underline{R})$ have to be connected by the convolution with the DCF $\hat{\rho}_{e,a}(R)$ of the spherical electronic environment of one atom:

$$\hat{\rho}_e(R)=\hat{\rho}_{e,a}(R)\otimes\hat{\rho}_a(\underline{R}) \tag{4}$$

The atomic density difference function (DDF) $\Delta\hat{\rho}_a(\underline{R})$, which is $\Delta\hat{\rho}_a(\underline{R})=\hat{\rho}_a(\underline{R})-\rho_0$ (ρ_0: mean density), is given by the Fourier transform of the reduced X-ray intensity $i_{red}(\underline{Q})$ (ref. 3).

$$\Delta\hat{\rho}_a(\underline{R})=\mathrm{F}^{-1}\{i_{red}(\underline{Q})\}$$

$$i_{red}(\underline{Q})=\frac{\mathrm{I}(\underline{Q})-\sum_{\mu=1}^{N} f_\mu^2(Q)}{f_e^2(Q)} \tag{5}$$

where $f_\mu^2(Q)$: scattering factor of atom μ and

$$f_e^2(Q)=\frac{\left(\sum_{\mu=1}^{N} f_\mu(Q)\right)^2}{\left(\sum_{\mu=1}^{N} Z_\mu\right)^2}$$

is the mean scattering factor per electron in which N is the number of atoms and Z_μ is the electronic charge of atom μ.

Now the orientation density distribution function (ODDF) $D(R, \alpha)$ is introduced. It indicates the relative frequency of finding any two atoms with the distance R to each other and the angle α with respect to the draw direction. This simplification is possible because the samples were drawn uniaxially and therefore showed a cylindrical symmetry:

$$D(R, \alpha)\sin\alpha\, d\alpha=[d\eta(R, \alpha)/\eta(R)] \tag{6}$$

$d\eta(R, \alpha)dR$ is the number of atoms lying within the angle $d\alpha$ and within the spherical shell of thickness dR (*Figure 4*). $d\eta(R, \alpha)$ is related to the atomic DCF $\hat{\rho}_a(R, \alpha)$ by

$$d\eta(R, \alpha)=2\pi R^2\hat{\rho}_a(R, \alpha)\sin\alpha\, d\alpha \tag{7}$$

$\eta(R)dR$ is the total number of atoms within the spherical shell of thickness dR.

$\eta(R)$ is given by

$$\eta(R)=\int_{\alpha=0}^{\alpha=\pi} d\eta(R, \alpha)=4\pi R^2\hat{\rho}_a(R) \tag{8}$$

with

$$\hat{\rho}_a(R)=1/2\int_0^{\pi}\hat{\rho}_a(R, \alpha)\sin\alpha\, d\alpha$$

The ODDF $D(R, \alpha)$ results from equation (6):

$$D(R, \alpha)=1/2[\hat{\rho}_a(R, \alpha)/\hat{\rho}_a(R)] \tag{9}$$

In a polymer material all atoms are part of macromolecules. Therefore the DCF $\hat{\rho}_a(R, \alpha)$ contains intramolecular as well as intermolecular correlations. The question arises which of the interatomic correlations mainly contribute to a specified halo. In order to calculate the real orientation distribution of the chain segments a concrete model of the molecular short range order which remains invariant during the deformation process has to be introduced.

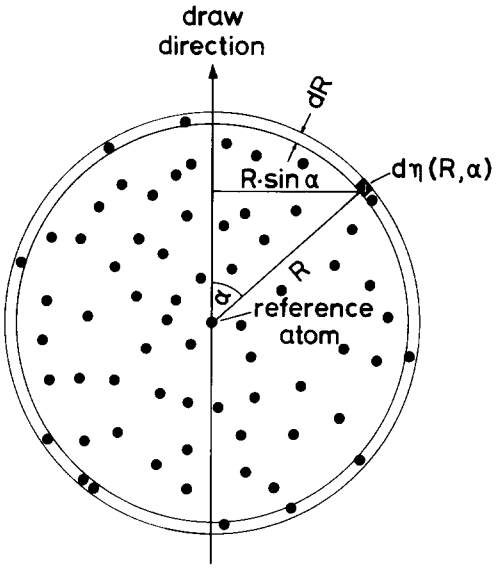

Figure 4 Schematic representation of the atomic orientation distribution for samples with cylindrical symmetry

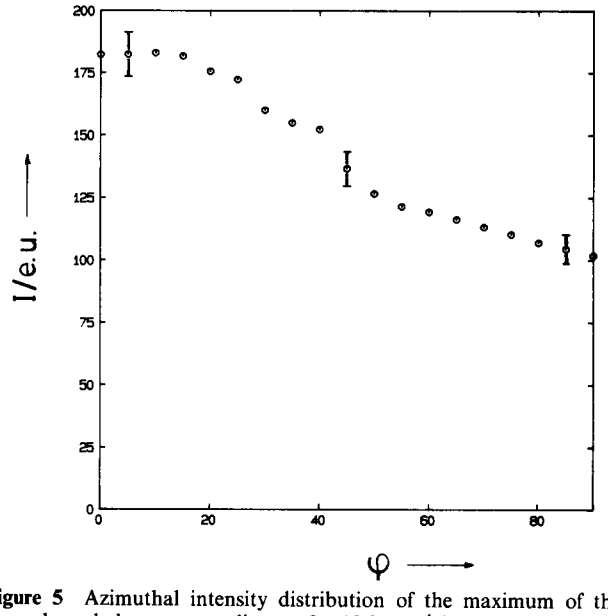

Figure 5 Azimuthal intensity distribution of the maximum of the amorphous halo corresponding to $Q\approx 13.0\,nm^{-1}$ in sample E, $\lambda=2.9$

As a first approximation it was assumed that the amorphous halo is mainly caused by intramolecular correlations. This was concluded from the fact that all measured azimuthal intensity distributions of the separated amorphous halo show a meridional maximum (see *Figure 5* as example).

Under this assumption the orientation parameter $\langle P_2\rangle$ describes the mean orientation of the chain segments and it can be calculated directly from the azimuthal intensity distribution by the well known relationship

$$\langle P_2\rangle_{am}=\frac{\int_0^{\pi/2}\frac{1}{2}(3\cos^2\varphi-1)I_{am}(Q, \varphi)\sin\varphi\, d\varphi}{\int_0^{\pi/2} I_{am}(Q, \varphi)\sin\varphi\, d\varphi} \tag{10}$$

$I_{am}(Q, \varphi)$ is the amorphous intensity, φ is the azimuthal angle.

Orientation of crystals

The mean orientation of an *hkl* plane with respect to a preferred direction Z can be described by

$$\begin{aligned}\langle\cos^2\Phi_{hkl,Z}\rangle = {} & e^2\langle\cos^2\Phi_{U,Z}\rangle + f^2\langle\cos^2\Phi_{V,Z}\rangle \\ & + g^2\langle\cos^2\Phi_{c,Z}\rangle \\ & + 2ef\langle\cos\Phi_{U,Z}\times\cos\Phi_{V,Z}\rangle \\ & + 2eg\langle\cos\Phi_{U,Z}\times\cos\Phi_{c,Z}\rangle \\ & + 2fg\langle\cos\Phi_{V,Z}\times\cos\Phi_{c,Z}\rangle \qquad (11)\end{aligned}$$

e, f and g are the direction cosines between the *hkl* normal vector and the a, b and c axes of the unit cell, respectively. $\Phi_{U,Z}$, $\Phi_{V,Z}$ and $\Phi_{c,Z}$ are the angles between a crystal fixed orthogonal coordinate system U, V, c with preferred direction $Z = c$. In an orthorhombic unit cell (as used for our samples) the last three terms of equation (11) average to zero.

To determine $\langle\cos^2\Phi_{c,z}\rangle$ and therefore the mean c-axis orientation, two reflections (1, 2) and three equations are needed:

$$\begin{aligned}\langle\cos^2\Phi_{1,Z}\rangle = {} & e_1^2\langle\cos^2\Phi_{U,Z}\rangle + f_1^2\langle\cos^2\Phi_{V,Z}\rangle \\ & + g_1^2\langle\cos^2\Phi_{cZ}\rangle \qquad (12)\end{aligned}$$

$$\begin{aligned}\langle\cos^2\Phi_{2,Z}\rangle = {} & e_2^2\langle\cos^2\Phi_{U,Z}\rangle + f_2^2\langle\cos^2\Phi_{V,Z}\rangle \\ & + g_2^2\langle\cos^2\Phi_{c,Z}\rangle \qquad (13)\end{aligned}$$

$$\begin{aligned}1 = {} & \langle\cos^2\Phi_{U,Z}\rangle + \langle\cos^2\Phi_{V,Z}\rangle \\ & + \langle\cos^2\Phi_{C,Z}\rangle \qquad (14)\end{aligned}$$

Equation (14) is the orthogonality relation.

$\langle\cos^2\Phi_{c,Z}\rangle$ is given by[7]:

$$\langle\cos^2\Phi_{c,Z}\rangle = \frac{\begin{vmatrix} e_1^2 & f_1^2 & \langle\cos^2\Phi_{1,Z}\rangle \\ e_2^2 & f_2^2 & \langle\cos^2\Phi_{2,Z}\rangle \\ 1 & 1 & 1 \end{vmatrix}}{\begin{vmatrix} e_1^2 & f_1^2 & g_1^2 \\ e_2^2 & f_2^2 & g_2^2 \\ 1 & 1 & 1 \end{vmatrix}} \qquad (15)$$

DETERMINATION OF CRYSTALLINITY

In the following, 'crystallinity' means 'weight fraction of two-dimensional ordered domains'. According to Ruland[8], the crystallinity of isotropic substances is given by

$$x_c = \frac{\int_0^\infty Q^2 I_{cr}(Q)\,dQ}{\int_0^\infty Q^2 I(Q)\,dQ} \times \underbrace{\frac{\int_0^\infty Q^2\overline{f^2}\,dQ}{\int_0^\infty Q^2\overline{f^2}D\,dQ}}_{K} \qquad (16)$$

where $I_{cr}(Q)$ is X-ray intensity of the crystal reflections; $I(Q)$, whole X-ray intensity and

$$\overline{f^2} = \sum_i N_i f_i^2 / \sum_i N_i$$

f_i^2: scattering factor of an atom of type i

N_i: number of atoms of type i

D: 'disorder' function

In the case of cylindrical symmetry only the angular integration in reciprocal space around the drawing axis can be performed. The result for $x_{c,cyl}$ is:

$$x_{c,cyl} = \frac{\int_0^\infty\int_0^{\pi/2} Q^2 I_{cr}(Q,\varphi)\sin\varphi\,d\varphi dQ}{\int_0^\infty\int_0^{\pi/2} Q^2 I(Q,\varphi)\sin\varphi\,d\varphi dQ} K \qquad (17)$$

$K = 1$ (no disorder) was taken as first approximation. The infinite integration in Q space was replaced by a finite integration from Q_{min} to Q_{max}, which are identical to the Q range of the separation procedure.

RESULTS AND DISCUSSION

In *Figure 6* the two-dimensional X-ray diffraction pattern of sample B is shown, meridional and equatorial scans are shown in *Figure 7*. The unit cells of all samples were assumed to be orthorhombic with $a = 0.857$ nm,

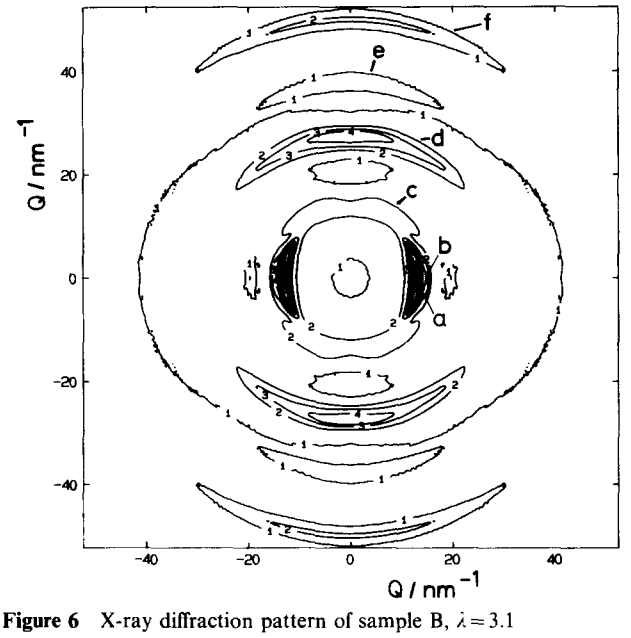

Figure 6 X-ray diffraction pattern of sample B, $\lambda = 3.1$

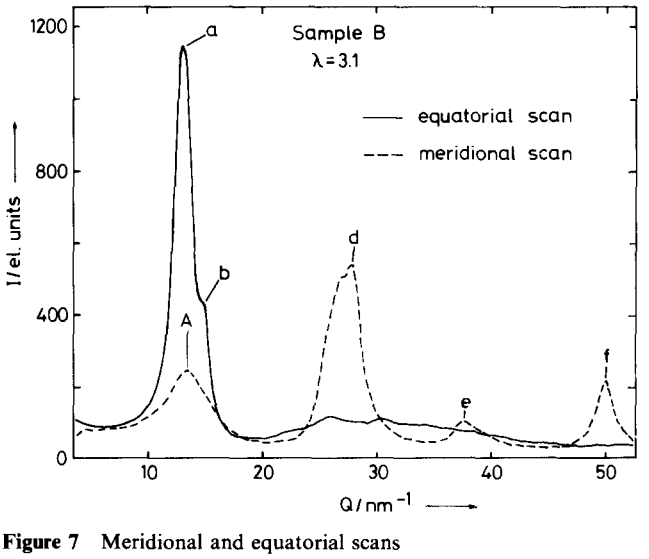

Figure 7 Meridional and equatorial scans

$b=1.120$ nm and $c=0.504$ nm (ref. 9). In previous publications, other values were given for the cell parameters, for example $a=0.960$ nm, $b=0.925$ nm, $c=0.504$ nm, $\gamma=96°$ (ref. 10). It was not possible to determine the unit cell from the X-ray data observed because of the missing *hkl* reflections.

Another way to obtain information about the unit cell is to examine the crystal orientation behaviour. We tried to determine the crystal orientation parameters using the unit cell suggested by Wilson and Starkweather[10] but this was not practicable because the orientation of the *c*-axis obtained in this way showed no continuous course. A continuous deformation should, however, produce a continuous orientation behaviour of the *c*-axis. In *Table 2* the Miller indices of reflections a–f are listed.

The separation procedure has been carried out to separate reflections a–c from the 'amorphous halo' A.

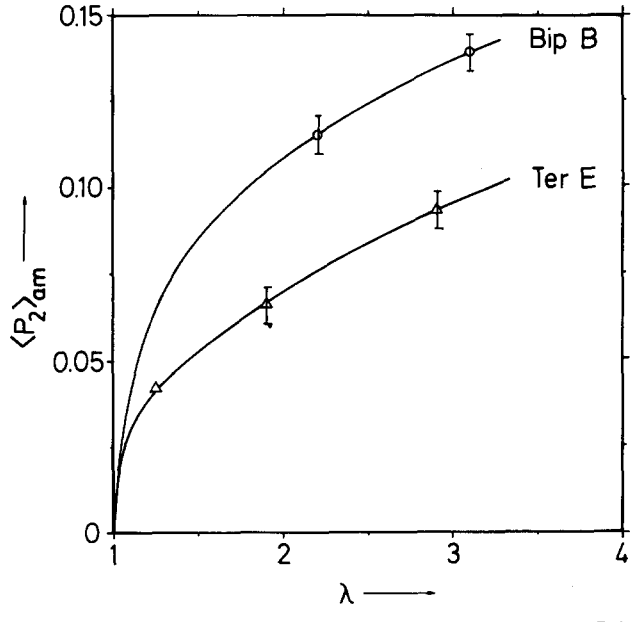

Figure 8 Typical behaviour of the orientation parameter $\langle P_2\rangle_{am}$ determined by equation (10). The error bars are caused mainly by statistical errors of the separation procedure

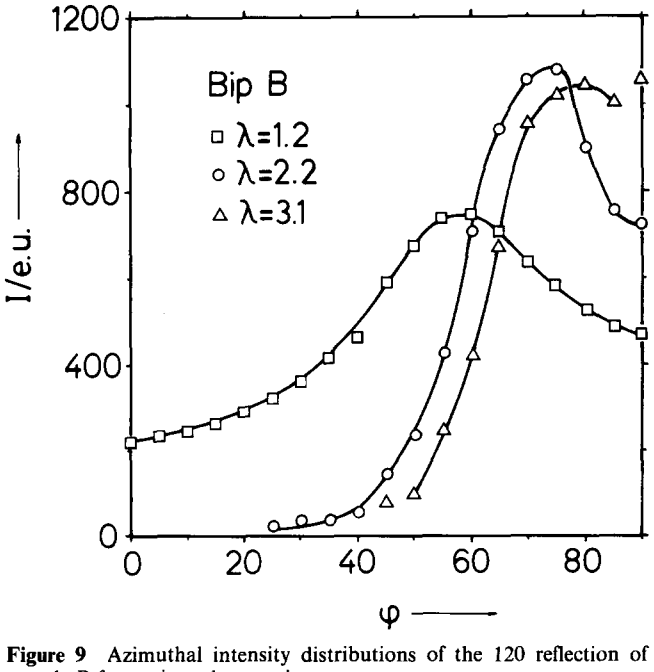

Figure 9 Azimuthal intensity distributions of the 120 reflection of sample B for various draw ratios

Table 2 Miller indices of reflections a–f and orientation maxima assuming perfect orientation

Reflection	Q_o (nm^{-1})	Orientation (°)	Miller indices
A	13.0	0	amorphous halo
a	13.4	90	120
b	14.7	90	200
c	15.5	36.5	111
d	28.0	0	002
e	37.4	0	003
f	49.9	0	004

Table 3 Draw ratios, orientation parameters $\langle P_2\rangle_{am}$ and crystallinities

Sample	λ	$\langle P_2\rangle_{am}$	x_c (mol%)
Bip B	1	0	0.328
	1.2	–	0.419
	2.2	0.115	0.443
	3.1	0.139	0.446
Qua C	1	0	0.282
	1.9	0.083	0.357
	2.1	0.086	0.383
Qua D	1	0	0.241
	2.4	0.117	0.419
Ter E	1	0	0.266
	1.25	0.042	0.303
	1.9	0.066	0.330
	2.9	0.093	0.347
Qua F	1	0	0.228
	2.3	0.116	0.419
Ter G	1	0	0.278
	3.5	0.114	0.395

Reflections d–f are of intramolecular origin and were not analysed further. Then, $\langle P_2\rangle_{am}$ has been calculated using equation (10). The maximum value of $\langle P_2\rangle_{am}$ at $Q\approx 13.0\,\text{nm}^{-1}$ corresponding to distances of about 0.48 nm is plotted v. the draw ratio for samples B and E in *Figure 8*.

As indicated before, it was assumed that all orientation parameters $\langle P_2\rangle_{am}$ are related to the chain segments. This means that mainly intramolecular correlations corresponding to distances of about 0.48 nm contribute to the amorphous halo. In comparison, the contributions of intermolecular correlations are small. The amorphous orientation in sample E is smaller than in sample B. Looking at the other samples (see *Table 3*), $\langle P_2\rangle_{am}$ remains nearly constant at comparable draw ratios. This behaviour is caused by the fact that the side chains contribute to equatorial X-ray scattering thus lowering the orientation parameter. No explanation can be given for why this happens only for sample E.

Next, the orientation distribution of the *ab* lattice planes was determined at various draw ratios using the azimuthal intensity distribution of reflection a. The result for sample B is shown in *Figure 9*. The orientation behaviour of the crystals with respect to the draw direction *V* is characterized by the orientation parameters f_a, f_b and f_c in *Figure 10*.

f_i was calculated using equation (15) and

$$f_i=1/2(3\langle\cos^2\Phi_{i,V}\rangle-1) \qquad (18)$$

Samples B, C and E (these were the samples with rather strong 200 reflections) show no difference in crystalline orientation behaviour. The crystallographic *a* axis tilts nearly perpendicular to the draw direction at $\lambda\approx 1.2$ and remains in this orientation state while the *c* axis moves

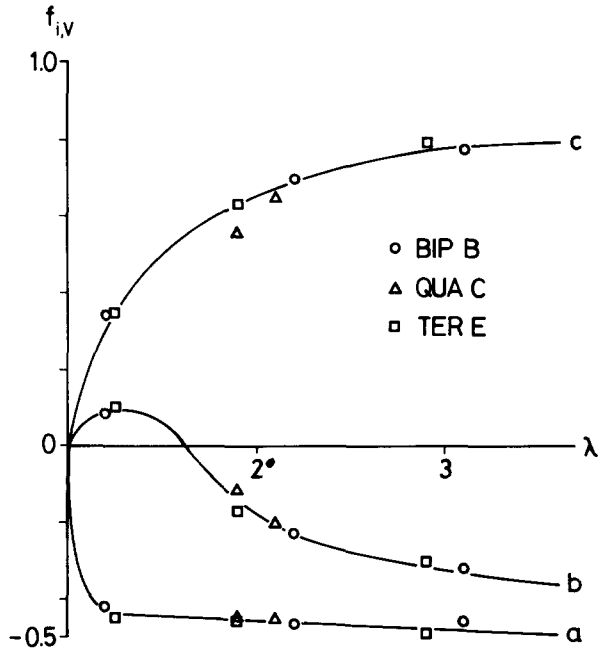

Figure 10 Orientation behaviour of the crystallographic axes with respect to the draw direction

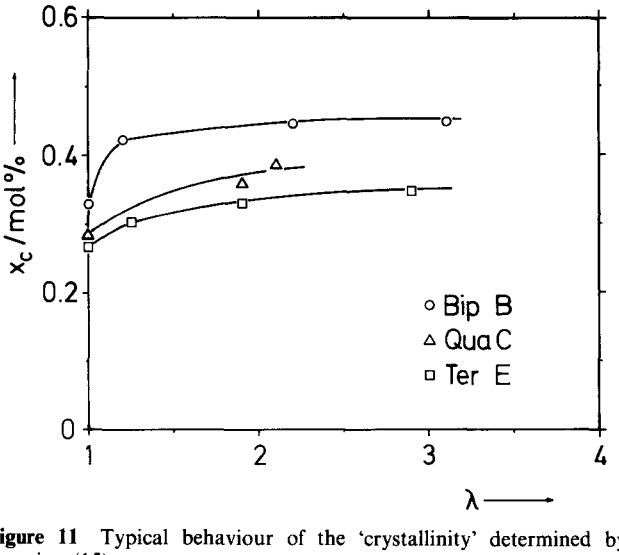

Figure 11 Typical behaviour of the 'crystallinity' determined by equation (15)

simultaneously into the draw direction. These effects cause the mean orientation parameter of the *b* axis to be positive at $\lambda \approx 1.2$. With increasing draw ratio the *b* axis moves slowly perpendicular to the draw direction. The mean angle of the *c* axis with the draw direction is about 21 degrees ($f_c = 0.8$) before the sample breaks.

The crystallinity was determined using equation (17). x_c is generally increased by strain induced crystallization which changes amorphous material into crystals (*Figure 11*).

The crystallinity decreases with increasing side chain amount because the side chains are not built into the crystals on account of their size.

The perfection of three-dimensional crystals increases by strain induced longitudinal rearrangement of the chains causing *hkl* reflections in the X-ray pattern. This has only been observed in sample B.

Tanigami *et al.*[11] observed a peculiar behaviour of the thermal expansion of the ETFE unit cell at about 100°C. They explained this anomaly with a crystal transition from an orthorhombic phase to a hexagonal phase which they called 'mesophase'. In this study, unoriented ETFE samples were examined in the temperature range of 50–300°C. Because of the overlapping of 200 and 120 reflections in our samples only one reflection could be observed. In the following this reflection will be called 100 reflection according to ref. 11. The corresponding net plane spacings were calculated with $d_{100} = 2\pi/Q_{100}$ (Q_{100} is the position of reflection 100 in Q space) and are plotted vs. temperature in *Figure 12a-g*. If we follow the interpretation of Tanigami *et al.*[11] the following can be stated.

Samples A and B (unmodified samples) show similar behaviour. The d_{100} spacings decrease up to $T = 100$°C where they reach a minimum. Above this temperature a 'normal' thermal expansion can be observed. According to Tanigami *et al.*[11], the orthorhombic crystals 'use' the thermal energy in order to reach an energetic lower state which is obviously the hexagonal packing mode. The *a* axis increases and the *b'* axis ($b' = b/2$) decreases until $b/a = \sqrt{3}$. Above $T = 100$°C the anharmonicity of the chain–chain potential predominates and the unit cell expands.

Samples C–G (modified samples; see *Table 1*) also show similar behaviour. The d_{100} spacings, which hardly differ from one another, increase continuously with increasing temperature. Obviously the side chain modifications enable the molecules to form the hexagonal lattice using less energy than the unmodified systems.

In *Figure 13* the mean lateral extension $\bar{D}_{lat}$ of the pseudo-hexagonal crystals is plotted vs. temperature. $\bar{D}_{lat}$ has been calculated directly from the integral line widths using $\bar{D}_{lat} = 2\pi/\delta\beta$. No corrections for instrumental line broadening were made. Therefore, the values of $\bar{D}_{lat}$ are lower limits. Again, a transition can be observed on sample A. Above $T = 100$°C the crystal extensions in the samples A and E are nearly the same, below 100°C the difference is about 2.5 nm.

CONCLUSIONS

The orientation parameters of the *a*, *b* and *c* axes (*Figure 10*) show similar behaviour to the orientation parameters of PE (ref. 12, 13). In particular the difference of the *a* and *b* axis orientation points to the existence of a lamellar structure analogous to PE. A further reference to a lamellar structure follows from SAXS investigations because temperature-dependent measurements show the occurrence of a long period[14]. The values of f_c in ETFE are smaller than those in PE. This is probably due to the smaller amount of crystallinity.

The orientation of the amorphous chain segments (*Figure 8*) shows the same behaviour for all samples with the exception of sample E. Model calculations for constrained chains in semicrystalline polymers have been performed in detail[15]. These calculations show that the orientation is determined essentially by tie chains. Also, the orientation is a function of both the interlamellar spacing and the segment number of the interlamellar amorphous chains. The interlamellar spacing depends on the deformation state and the crystallinity. Therefore, $\langle P_2 \rangle_{am}$ is determined by these effects, because the segment number changes with the crystallinity. The superstructure of our samples is still unknown, therefore a quantitative discussion of $\langle P_2 \rangle_{am}$ on the basis of a structure model is impossible at present.

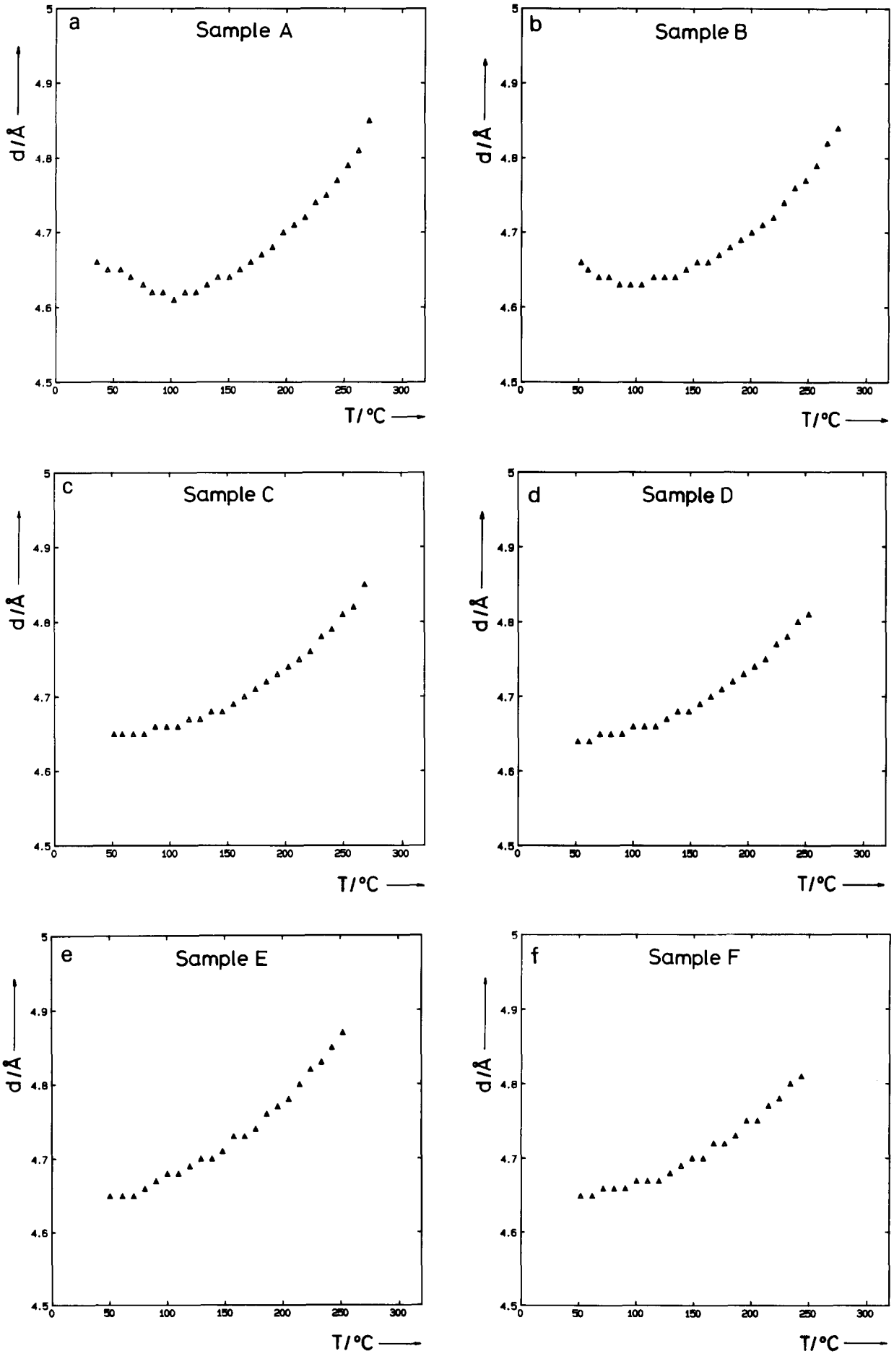

Figure 12 a–g Mean lattice constants in A of samples A–G. The anomaly of samples A and B at 100°C is attributed to a transition of the 'crystal' structure

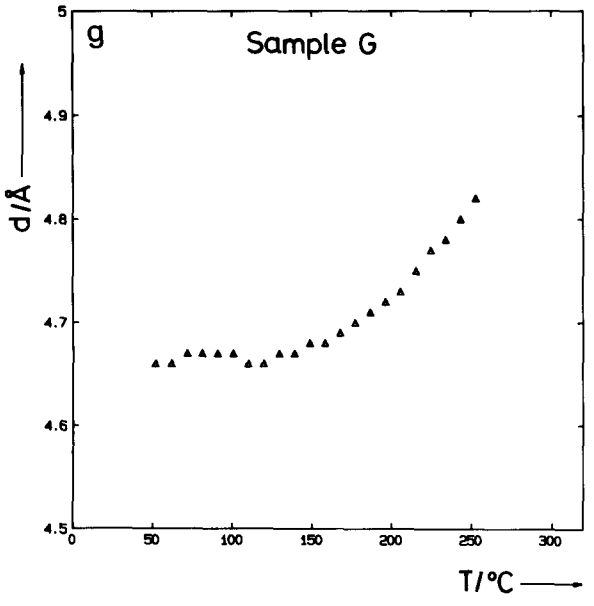

Figure 12 *(continued)*

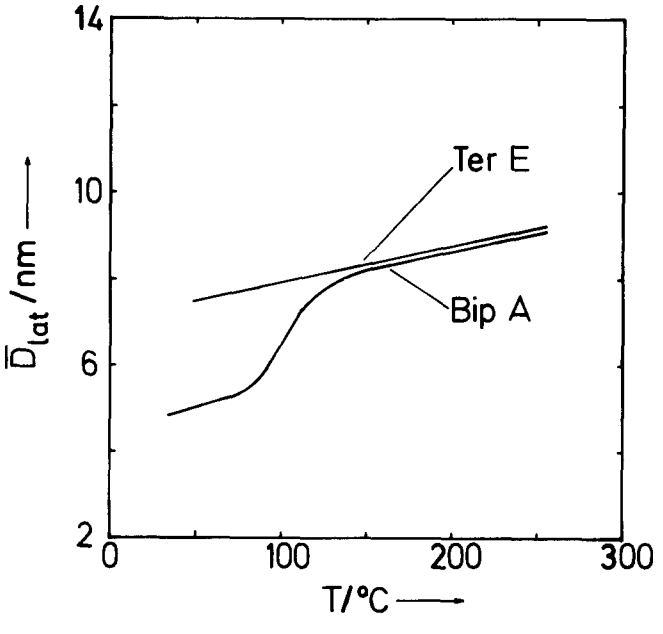

Figure 13 Mean lateral extension of the coherent scattering domains. The values were calculated directly from the experimental X-ray data, i.e. no corrections for instrumental line broadening were made

With respect to the crystal orientation sample E behaves like all other samples. This is not the case with the orientation of the amorphous regions. $\langle P_2 \rangle_{am}$ lies below the values of the other samples. This different behaviour is also expressed in the stress–strain curves. The yield stress of sample E and the further course of the stress–strain curve lies about 20% below the corresponding values of the other samples[16].

At $T \approx 100°C$ the unmodified samples perform a crystal transition from orthorhombic to hexagonal. This behaviour corresponds with results of Tanigami *et al.*[11] in ETFE crystals with higher crystalline perfection. Obviously the disorder caused by longitudinal chain displacement does not affect the lateral chain packing and the associated phase transition. In the presence of side chains only the hexagonal phase can be observed.

ACKNOWLEDGEMENTS

This work was funded by the German Federal Ministry for Research and Technology (BMFT) under the contract number 05 379AX B 4. The authors wish to thank Hoechst AG for providing the sample material and for good cooperation within the BMFT project 03C 179 0.

REFERENCES

1 Modena, M., Garbuglio, C. and Ragazzini, M. *Polym. Lett.* 1972, **10**, 153
2 Garbuglio, C., Modena, M., Valera, M. and Ragazzini, M. *Eur. Polym. J.* 1974, **10**, 91
3 Schubach, H. R. and Heise, B. *Coll. Polym. Sci.* 1986, **264**, 335
4 Schubach, H. R., Nagy, E. and Heise, B. *Coll. Polym. Sci.* 1981, **259**, 789
5 Dwiggins, C. W. Jr *Acta Cryst.* 1972, **A28**, 155
6 Hall, M. M. Jr, Veeraraghavan, V. G., Rubin, H. and Winchell, P.G. *J. Appl. Cryst.* 1977, **10**, 66
7 Alexander, L. E. 'X-Ray Diffraction Methods in Polymer Science', John Wiley, New York (1969)
8 Ruland, W. *Acta Cryst.* 1961, **14**, 1180
9 Tanigami, T., Yamaura, K., Matsuzawa, S., Ishikawa, M., Mizoguchi, K. and Miyasaka,K. *Polymer* 1986, **27**, 999
10 Wilson, F. C., Starkweather, H. W. Jr *J. Polym. Sci. Polym. Phys. Edn.* 1973, **11(5)**, 919
11 Tanigami, T., Yamaura, K., Matsuzawa, S., Ishikawa, M., Mizoguchi, K. and Miyasaka, K. *Polymer* 1986, **27**, 1521
12 Heise, B., Kilian, H. G. and Pietralla, M. *Prog. Coll. Polym. Sci.* 1977, **62**, 16
13 Oda, T., Nomura, S. and Kawai, H. *J. Polym. Sci. A* 1965, **3**, 1993
14 German Federal Ministry for Research and Technology (BMFT) Project Report 'Fluorpolymer-Composites', September 1988
15 Petraccone, V., Sanchez, I. C. and Stein, R. S. *J. Polym. Sci. Polym. Phys. Edn.* 1975, **13**, 1991
16 Schrodi, W. T. *Diplomarbeit*, University of Ulm, 1985